Hindawi
Advances in High Energy Physics
Volume 2018, Article ID 1260124, 9 pages
https://doi.org/10.1155/2018/1260124

Research Article

Angular Dependence of η Photoproduction in Photon-Induced Reaction

Jun-Zhen Wang and Bao-Chun Li

Department of Physics, Shanxi University, Taiyuan, Shanxi 030006, China

Correspondence should be addressed to Bao-Chun Li; libc2010@163.com

Received 23 April 2018; Accepted 13 September 2018; Published 30 September 2018

Guest Editor: Sakina Fakhraddin

Photoproduction of η mesons from nucleons can provide valuable information about the excitation spectrum of the nucleons. The angular dependence of η photoproduction in the photon-induced reaction is investigated in the multisource thermal model. The results are compared with experimental data from the $\eta \longrightarrow 3\pi^0 \longrightarrow 6\gamma$ decay mode. They are in good agreement with the experimental data. It is shown that the movement factor increases linearly with the photon beam energies. And the deformation and translation of emission sources are visually given in the formalism.

1. Introduction

The excitation spectrum of nucleons is important to understanding the nonperturbative behavior of the fundamental theory of strong interactions, Quantum Chromodynamics (QCD) [1–4]. The photon-induced meson production off nucleons is mainly used to achieve more information from the excitation spectrum of nucleons. It is very important for missing resonances that the η meson production in photon-induced and hadron-induced reactions on free (and quasi-free) nucleons and on nuclei [5–8]. The advantage of photon-induced reactions is that the electromagnetic couplings can provide valuable information related to the details of the model wave functions. Because the electromagnetic excitations are isospin dependent, we need perform meson-production reactions off the neutron.

Recently, the photoproduction of η mesons from quasi-free protons and neutrons was measured in $\eta \longrightarrow 3\pi^0 \longrightarrow 6\gamma$ decay mode by the CBELSA/TAPS detector at the electron accelerator ELSA in Bonn [9]. At different incident photon energies, the experiments are performed by the incident photon beam on a liquid deuterium target. A great number of η mesons are produced in the photon-induced reaction. The experimental data are regarded as a multiparticle system. And, their angular distributions represent an obvious regularity at different incident photon energies. In order to explain the abundant experimental results, some statistical methods are proposed and developed [10–16]. In this work, we will extend a multi-source thermal model to the statistical investigation of the angular distributions in the photon-induced reaction and try to understand the η photoproduction in the reaction. In our previous wok [17–21], the model was focused on the investigation of the particle production in intermediate-energy and high-energy collisions.

2. η Meson Distribution in the Multi-Source Thermal Model

In the multi-source thermal model [17–21], many emission sources are expected to be formed at the final stage of the photon-induced reaction. Every source emits particles isotropically in the source rest frame. The observed η mesons are from different emission sources. The incident beam direction is defined as an oz axis and the reaction plane is defined as yoz plane. In the source rest frame, the meson momentum p_x, p_y, and p_z obeys a normal distribution. The corresponding transverse momentum $p_T = \sqrt{p_x^2 + p_y^2}$ obeys a Rayleigh distribution:

$$f_{p_T}(p_T) = \frac{p_T}{\sigma^2} e^{-p_T^2/2\sigma^2}, \quad (1)$$

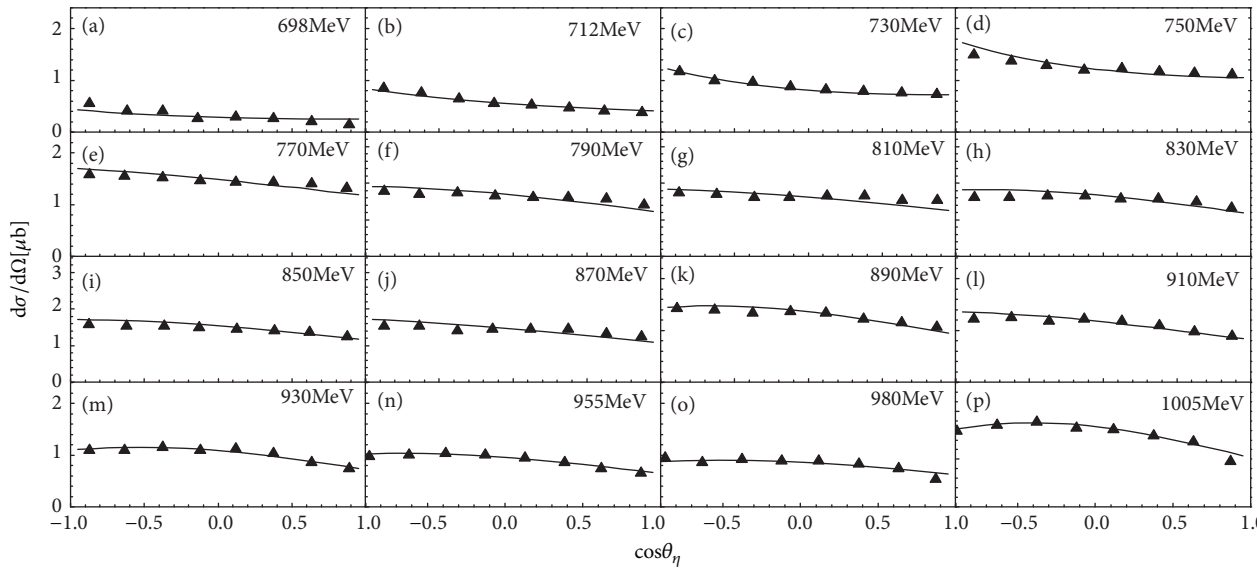

Figure 1: Angular distributions for different bins of incident photon energy 698 MeV ≤ E_γ ≤ 1005MeV as a function of $\cos\theta_\eta$ in the beam-target cm system assuming the initial state nucleon at rest. The symbols represent the experimental data from the CBELSA/TAPS detector at the electron accelerator ELSA in Bonn [9]. The results in the multi-source thermal model are shown with the curves.

where σ represents a distribution width. The distribution function of the polar angle θ is

$$f_\theta(\theta) = \frac{1}{2}\sin\theta \tag{2}$$

Because of the interactions with other emission sources, the considered source deforms and translates along the oz axis. Then, the momentum component is revised to

$$p_z' = a_z p_z + b_z\sigma \tag{3}$$

where a_z and b_z represent the coefficients of the source deformation and translation along the oz axis, respectively. The mathematical description of the deformable translational source is formulized simply as a linear relationship between p_z' and p_z, which reflects the mean result of the source interaction. For $a_z \neq 1$ or $b_z \neq 0$, the p_z' distribution of η mesons is anisotropic along the oz axis.

By using Monte Carlo method, p_T and p_z' are given by

$$p_T = \sigma\sqrt{-2\ln r_1}, \tag{4}$$

$$p_z' = a_z\sigma\sqrt{-2\ln r_2}\cos(2\pi r_3) + b_z\sigma, \tag{5}$$

where r_1, r_2, and r_3 are random numbers from 0 to 1. The polar angle θ is revised to

$$\theta' = \arctan\frac{p_T}{p_z'} = \arctan\frac{\sqrt{-2\ln r_1}}{a_z\sqrt{-2\ln r_2}\cos(2\pi r_3) + b_z}. \tag{6}$$

We can calculate a new distribution function of the polar angle by this formula.

3. Angular Dependencies of η Photoproduction in the Photon-Induced Reaction

Figures 1(a)–1(p) show the angular distributions of η mesons for different bins of incident photon energy 698 MeV ≤ E_γ ≤ 1005 MeV as a function of $\cos\theta_\eta$. θ_η is the polar angle of η meson in the beam-target cm system assuming the initial state nucleon at rest. The symbols represent the experimental data from the CBELSA/TAPS detector at the electron accelerator ELSA in Bonn [9]. The results obtained by using the multi-source thermal model are shown with the curves, which behave in the same way as the experimental data in the 16 bins of incident photon energy. By minimizing χ^2 per degree of freedom (χ^2/dof), we determine the corresponding parameters a_z and b_z, which are presented in Table 1. It is found that there is an almost linear relationship between the b_z and E_γ. As representative energies of Figure 1, we give a schematic sketch of these emission sources at the four different energies in Figure 7(a). The deformations and translations can be seen intuitively in the figure.

In Figures 2(a)–2(p) and Figures 3(a)–3(p), we present the angular distributions of η mesons for different bins of incident photon energy 1035 MeV ≤ E_γ ≤ 1835 MeV as a function of $\cos\theta_\eta$. θ_η is the polar angle of η meson in the beam-target cm system assuming the initial state nucleon at rest. Same as Figure 1, the symbols represent the experimental data from the CBELSA/TAPS detector at the electron accelerator ELSA in Bonn [9]. The results obtained by using the multisource thermal model are shown with the curves, which behave in the same way as the experimental data in the 28 bins of incident photon energy. Parameters a_z and b_z are presented in Tables 2 and 3. As the representative energies of Figures 1 and

Table 1: Values of a_z and b_z taken in Figure 1 model results.

Figure 1	E_γ (MeV)	a_z	b_z	χ^2/dof
(a)	698	1.050	-0.170	0.118
(b)	712	1.020	-0.210	0.105
(c)	730	1.050	-0.170	0.090
(d)	750	1.040	-0.155	0.134
(e)	770	0.985	-0.105	0.182
(f)	790	0.970	-0.125	0.179
(g)	810	0.979	-0.110	0.194
(h)	830	0.960	-0.120	0.192
(i)	850	0.970	-0.110	0.200
(j)	870	0.980	-0.130	0.211
(k)	890	0.950	-0.120	0.175
(l)	910	0.970	-0.140	0.261
(m)	930	0.940	-0.110	0.179
(n)	955	0.950	-0.120	0.154
(o)	980	0.950	-0.090	0.138
(p)	1005	0.920	-0.110	0.150

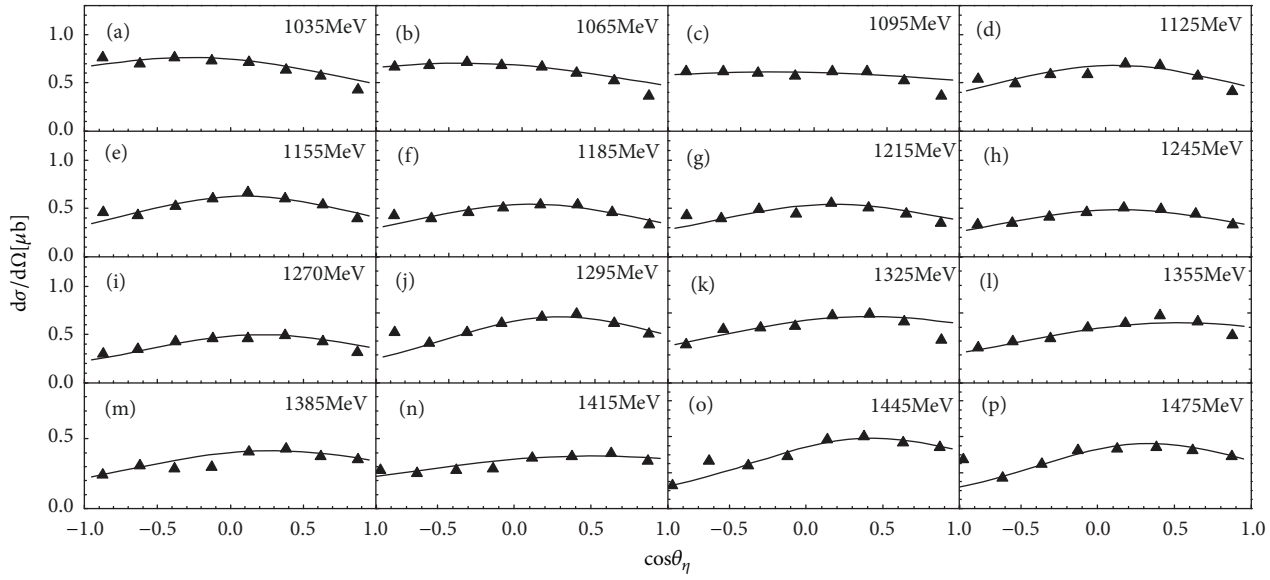

Figure 2: Same as Figure 1, but showing angular distributions for different bins of incident photon energy 1035 MeV ≤ E_γ ≤ 1475MeV.

2, the schematic sketches of the emission sources are given at different energies in Figures 7(b) and 7(c).

In Figures 4, 5, and 6, we show angular distributions in the η-nucleon cm system for $\gamma p \longrightarrow p\eta$ reaction for the different bins of final state energy 1488 MeV ≤ W ≤ 1625 MeV, 1635 MeV ≤ W ≤ 1830 MeV and 1850 MeV ≤ W ≤ 2070 MeV, respectively. Same as Figure 1, the model results and experimental data are indicated by the curves and symbols, respectively. The model results can also agree with the experimental data. In the same way, the deformations and translations of these emission sources are given in Tables 4–6 and Figures 7(d)–7(f). All the parameter values taken in the above calculations are also given in Figures 8 and 9. It can be found that a_z keeps almost invariable and fluctuates around 1.0 with the increasing E_γ. The parameter b_z increases linearly with the increasing E_γ and their relationship can be expressed by a linearly function, $b_z = (0.541 \pm 0.005) \times 10^{-3} E_\gamma - (0.622 \pm 0.011)$. There are similar relationships between the parameters and different final state energies W in Figure 9, where the fitting function of b_z is $b_z = (0.808 \pm 0.003) \times 10^{-3} W - (1.322 \pm 0.007)$.

4. Discussion and Conclusions

The excitation spectrum of nucleons can especially help us to understand the strong interaction in the nonperturbative regime. Before, the hadron induced reactions is a main experimental method in the investigation. In the last two

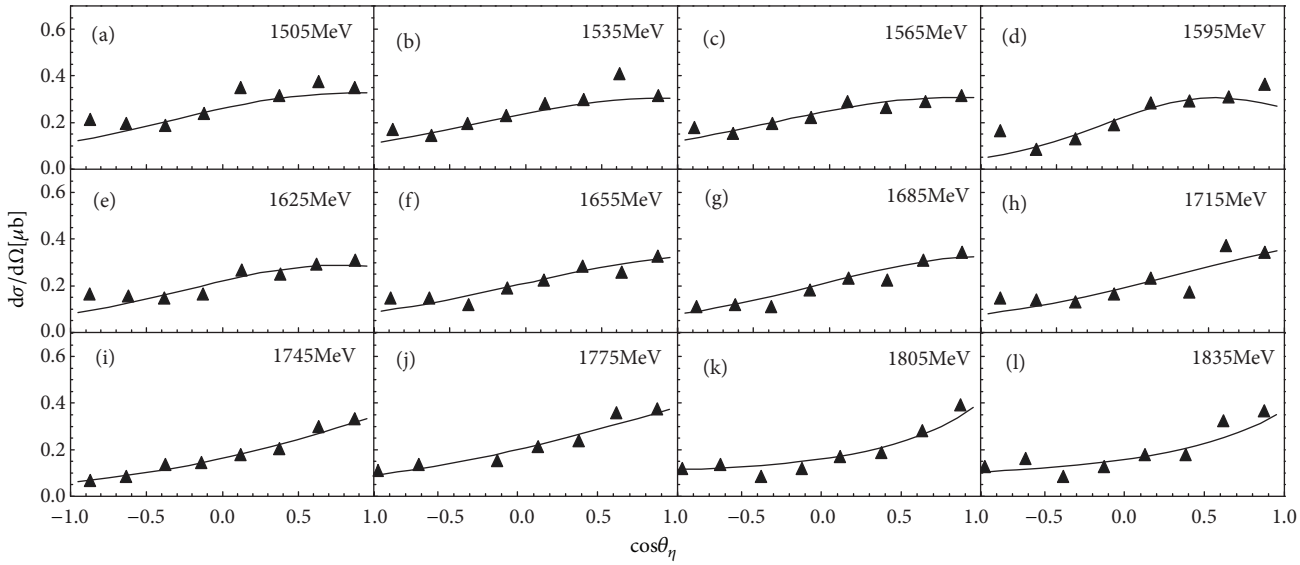

FIGURE 3: Same as Figure 1, but showing angular distributions for different bins of incident photon energy 1505 MeV ≤ E_γ ≤ 1835MeV.

TABLE 2: Values of a_z and b_z taken in Figure 2 model results.

Figure 2	E_γ (MeV)	a_z	b_z	χ^2/dof
(a)	1035	0.920	-0.080	0.124
(b)	1065	0.940	-0.090	0.118
(c)	1095	0.970	-0.030	0.132
(d)	1125	0.870	0.030	0.165
(e)	1155	0.850	0.050	0.170
(f)	1185	0.850	0.030	0.168
(g)	1215	0.860	0.070	0.173
(h)	1245	0.860	0.050	0.122
(i)	1270	0.850	0.110	0.121
(j)	1295	0.830	0.150	0.145
(k)	1325	0.910	0.120	0.147
(l)	1355	0.910	0.160	0.142
(m)	1385	0.890	0.110	0.115
(n)	1415	0.930	0.130	0.106
(o)	1445	0.830	0.250	0.122
(p)	1475	0.810	0.210	0.091

TABLE 3: Values of a_z and b_z taken in Figure 3 model results.

Figure 3	E_γ (MeV)	a_z	b_z	χ^2/dof
(a)	1505	0.915	0.260	0.243
(b)	1535	0.920	0.260	0.190
(c)	1565	0.920	0.240	0.158
(d)	1595	0.800	0.360	0.315
(e)	1625	0.890	0.310	0.179
(f)	1655	0.930	0.340	0.190
(g)	1685	0.910	0.360	0.206
(h)	1715	0.940	0.400	0.235
(i)	1745	0.960	0.460	0.085
(j)	1775	0.960	0.410	0.144
(k)	1805	1.090	0.400	0.132
(l)	1835	1.060	0.390	0.140

Table 4: Values of a_z and b_z taken in Figure 4 model results.

Figure 4	W (MeV)	a_z	b_z	χ^2/dof
(a)	1488	0.956	-0.098	0.086
(b)	1492	0.968	-0.069	0.125
(c)	1498	0.966	-0.058	0.101
(d)	1505	0.959	-0.063	0.114
(e)	1515	0.965	-0.052	0.205
(f)	1525	0.952	-0.048	0.192
(g)	1535	0.960	-0.063	0.143
(h)	1545	0.967	-0.066	0.206
(i)	1555	0.948	-0.060	0.174
(j)	1565	0.941	-0.072	0.168
(k)	1575	0.934	-0.059	0.170
(l)	1585	0.955	-0.068	0.235
(m)	1595	0.925	-0.051	0.260
(n)	1605	0.934	-0.039	0.251
(o)	1615	0.942	-0.045	0.307
(p)	1625	0.961	-0.058	0.293

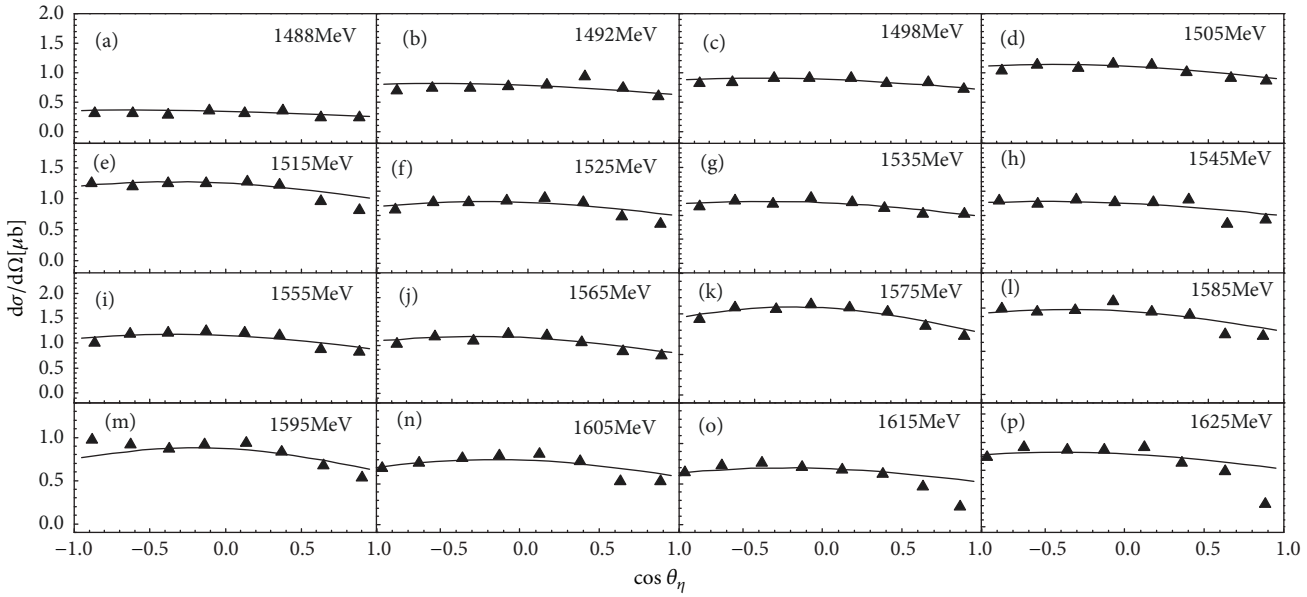

Figure 4: Angular distributions in the η-nucleon cm system for the reaction $\gamma p \longrightarrow p\eta$ for the different bins of final state energy 1488 MeV $\leq W \leq$ 1625 MeV. The symbols represent the experimental data from the CBELSA/TAPS detector at the electron accelerator ELSA in Bonn [9]. The results in the multisource thermal model are shown with the curves.

decades, the photon-induced reaction and electron scattering experiment are applied to study the electromagnetic excitation of baryons. Recently, the photoproduction of η mesons from quasi-free protons and neutrons are measured by the CBELSA/TAPS detector. In the paper, we theoretically study the angular distribution of η mesons for different incident photon energies E_γ and for different final state energies W. Then, the results are compared with the experimental data in detail. The deformation coefficient a_z and translation coefficient b_z are extracted by the comparison. a_z is almost independent of incident photon energies and final state energies. b_z is linearly dependent on incident photon energies and final state energies. In particular, we visually give the deformation and translation of the emission sources by schematic sketches. From the patterns, it is intuitive and easy to better understand the motion and configuration of the emission sources.

A great number of η mesons are produced in the photon-induced reaction. These η mesons are regarded as a multiparticle system, which can be analyzed by the statistical method. In recent years, we develop such a model, which is called multisource thermal model. Some emission sources of final-state particles are formed in the reaction. Each emission source emits particles isotropically in the rest frame of the emission

Table 5: Values of a_z and b_z taken in Figure 5 model results.

Figure 5	W (MeV)	a_z	b_z	χ^2/dof
(a)	1635	0.958	-0.042	0.305
(b)	1645	0.940	-0.028	0.350
(c)	1655	0.920	-0.021	0.263
(d)	1670	0.925	-0.009	0.187
(e)	1690	0.902	0.022	0.240
(f)	1710	0.899	0.047	0.209
(g)	1730	0.868	0.095	0.181
(h)	1750	0.843	0.102	0.194
(i)	1770	0.853	0.115	0.235
(j)	1790	0.879	0.125	0.170
(k)	1810	0.855	0.142	0.152
(l)	1830	0.867	0.159	0.138

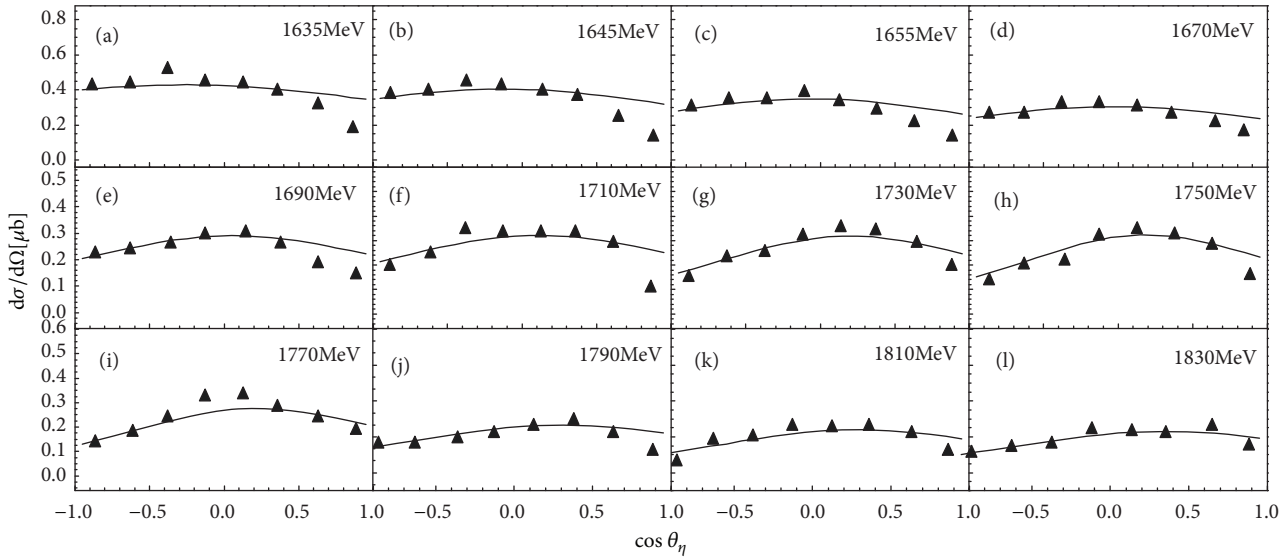

Figure 5: Same as Figure 4, but showing angular distributions for the different bins of final state energy 1635 MeV ≤ W ≤ 1830 MeV.

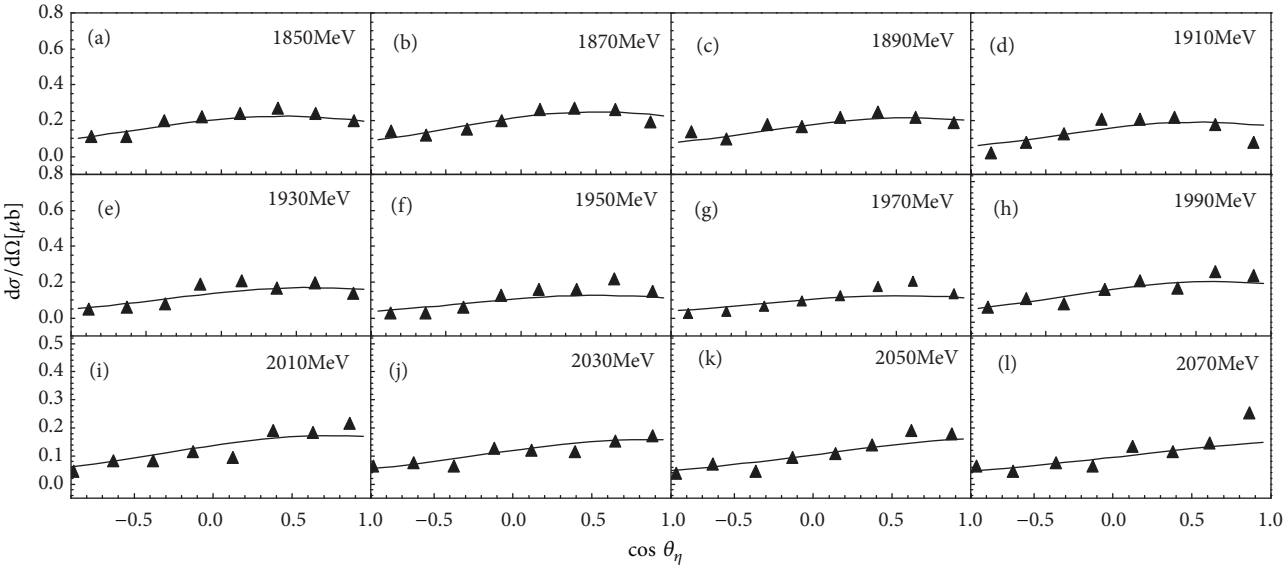

Figure 6: Same as Figure 4, but showing angular distributions for the different bins of final state energy 1850 MeV ≤ W ≤ 2070 MeV.

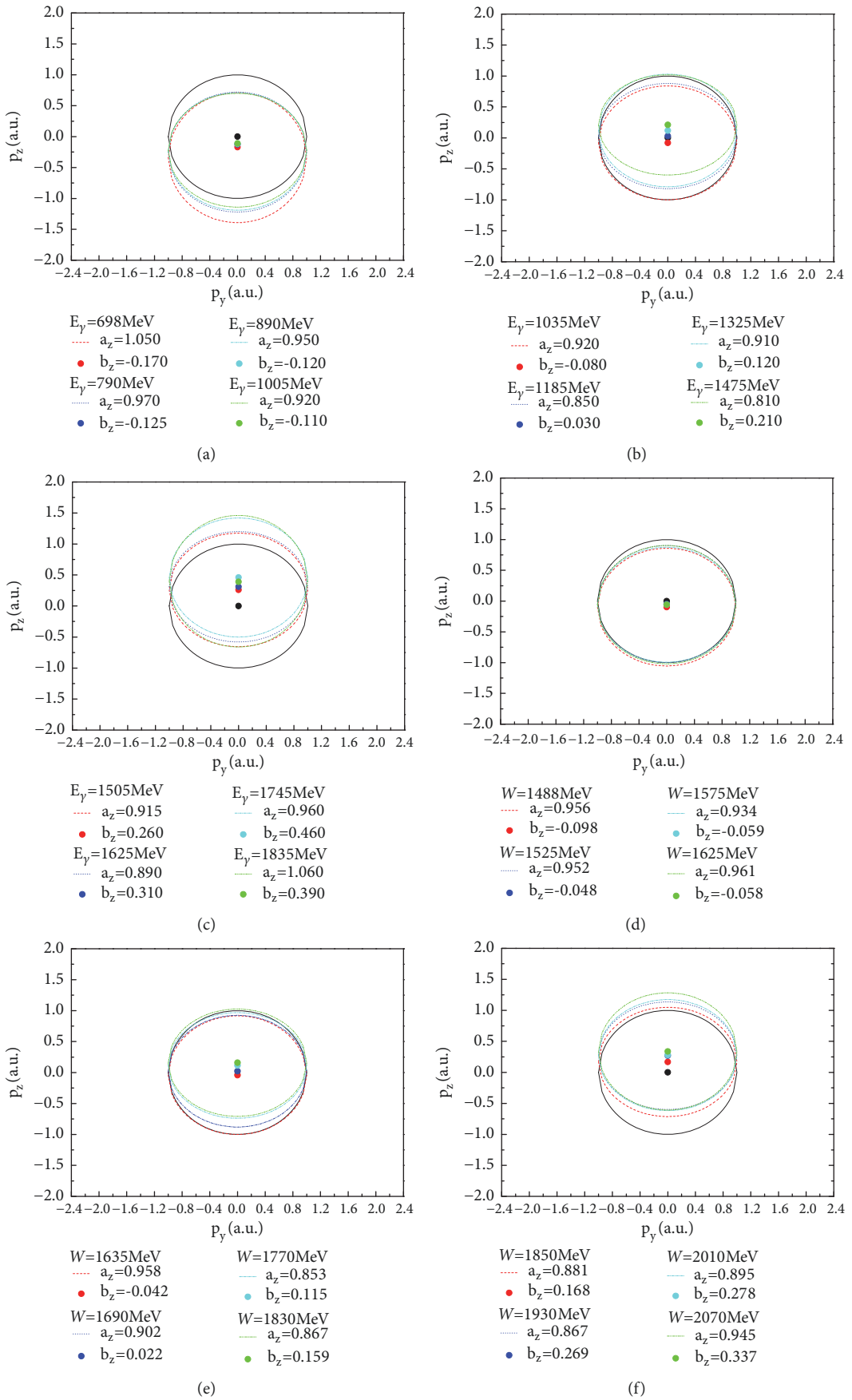

FIGURE 7: The deformable and translational source in the reaction plane for different bins of incident photon energy E_γ or final state energy W.

Table 6: Values of a_z and b_z taken in Figure 6 model results.

Figure 6	W (MeV)	a_z	b_z	χ^2/dof
(a)	1850	0.881	0.168	0.127
(b)	1870	0.872	0.221	0.132
(c)	1890	0.883	0.241	0.135
(d)	1910	0.856	0.252	0.153
(e)	1930	0.867	0.269	0.218
(f)	1950	0.853	0.253	0.295
(g)	1970	0.860	0.249	0.321
(h)	1990	0.875	0.261	0.184
(i)	2010	0.895	0.278	0.359
(j)	2030	0.906	0.299	0.337
(k)	2050	0.932	0.348	0.285
(l)	2070	0.945	0.337	0.304

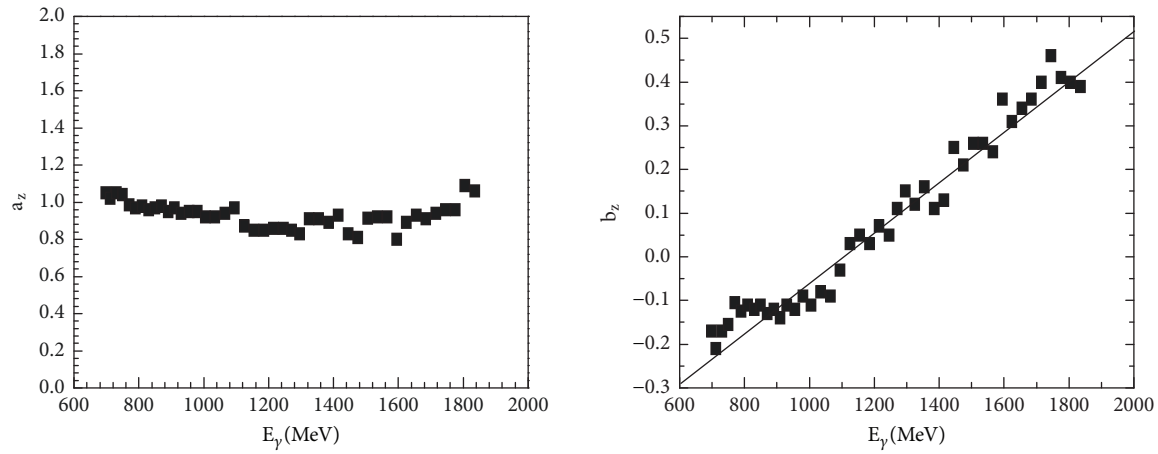

Figure 8: a_Z and b_Z for different bins of incident photon energy E_γ. The symbols are the values taken in Figures 1–3. The straight line is a fitted curve.

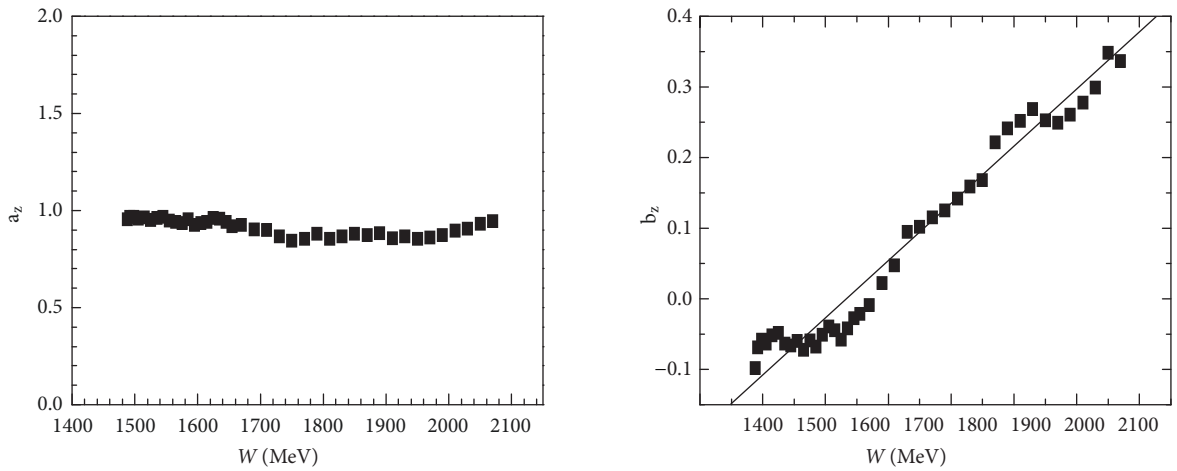

Figure 9: The a_Z and b_Z values taken for different bins of final state energy W. The symbols are the values taken in Figures 4–6. The straight line is a fitted curve.

source. Due to the source interaction, the sources emit particles anisotropically. The η mesons are emitted from these sources. In our previous work, the model can successfully describe transverse momentum spectra and pseudorapidity spectra of final-state particles produced in proton-proton (pp) collisions, proton-nucleus (pA) collisions, and nucleus -nucleus (AA) collisions at intermediate energy and at high energy [17–21]. In this work, we extend the multisource thermal model to the statistical investigation of final-state particles produced in the photon-induced reaction. The model is improved to describe the angular dependence of the η photoproduction from quasi-free protons and neutrons. The information of the source deformation and translation is obtained with different beam energies. It is helpful for us to understand the η photoproduction.

Data Availability

The theoretical results are compared with experimental data, which are from [9].

Conflicts of Interest

The authors declare that they have no conflicts of interest.

Acknowledgments

This work is supported by National Natural Science Foundation of China under Grants No. 11247250 and No. 11575103, Shanxi Provincial Natural Science Foundation under Grant No. 201701D121005, and Scientific and Technological Innovation Programs of Higher Education Institutions in Shanxi (STIP) Grant No. 201802017.

References

[1] B. Krusche, C. Wilkin, and Prog. Part, "Production of η and η' mesons on nucleons and nuclei," *Progress in Particle and Nuclear Physics*, vol. 80, pp. 43–95, 2014.

[2] M. Dieterle, "First measurement of the polarization observable E and helicity-dependent cross sections in single π^0 photoproduction from quasi-free nucleons," *Phys. Lett. B*, vol. 770, no. 523, 2017.

[3] B. C. Li, Y. Y. Fu, L. L. Wang, and F.-H. Liu, "Dependence of elliptic flows on transverse momentum and number of participants in Au+Au collisions at $\sqrt{s_{NN}}$=200 GeV," *Journal of Physics G: Nuclear and Particle Physics*, vol. 40, no. 2, Article ID 025104, 2013.

[4] T. Sekihara, H. Fujioka, and T. Ishikawa, "Possible η'd bound state and its bound state and its s-channel formation in the γd $\longrightarrow$ ηd reaction," *Physical Review C*, vol. 97, Article ID 045202, 2018.

[5] A. V. Anisovich, "Neutron helicity amplitudes," *Physical Review C*, vol. 96, Article ID 055202, 2017.

[6] V. Kuznetsov, "Observation of Narrow $N^+(1685)$ and N^o Resonances in $_\gamma N \longrightarrow \pi\eta N$ Reactions," *JETP Lett*, vol. 106, no. 11, pp. 693–699, 2017.

[7] J. D. Holt, J. Menéndez, J. Simonis, and A. Schwenk, "Three-nucleon forces and spectroscopy of neutron-rich calcium isotopes," *Physical Review C: Nuclear Physics*, vol. 90, no. 2, Article ID 024312, 2014.

[8] S. A. Voloshin, "Collective phenomena in ultra-relativistic nuclear collisions: anisotropic flow and more," *Progress in Particle and Nuclear Physics*, vol. 67, no. 2, pp. 541–546, 2012.

[9] L. Witthauer, "Photoproduction of η mesons from the neutron: Cross sections and double polarization observable E," *The European Physical Journal A*, vol. 53, no. 58, 2017.

[10] J. Rafelski and J. Letessier, "Testing limits of statistical hadronization," *Nuclear Physics A*, vol. 715, p. 98, 2003.

[11] A. Andronic, P. Braun-Munzinger, and J. Stachel, "Thermal hadron production in relativistic nuclear collisions: The hadron mass spectrum, the horn, and the QCD phase transition," *Physics Letters B*, vol. 673, no. 2, pp. 142–145, 2009.

[12] J. Cleymans, H. Oeschler, K. Redlich, and S. Wheaton, "Comparison of chemical freeze-out criteria in heavy-ion collisions," *Physical Review C: Nuclear Physics*, vol. 73, no. 4, Article ID 034905, 2006.

[13] P. Braun-Munzinger, J. Stachel, and C. Wetterich, "Chemical freeze-out and the QCD phase transition temperature," *Physics Letters B*, vol. 596, no. 1-2, pp. 61–69, 2004.

[14] A. Adare, S. Afanasiev, and C. Aidala, "Measurement of neutral mesons in p+p collisions at $\sqrt{s}$=200 GeV and scaling properties of hadron production," *Physical Review D: Particles, Fields, Gravitation and Cosmology*, vol. 83, Article ID 052004, 2011.

[15] K. Aamodt, N. Abel, and U. Abeysekara, "Transverse momentum spectra of charged particles in proton–proton collisions at $\sqrt{s}$ = 900 GeV with ALICE at the LHC," *Physics Letters B*, vol. 693, no. 2, pp. 53–68, 2010.

[16] C. Y. Wong and G. Wilk, "Tsallis fits to p_T spectra and multiple hard scattering in pp collisions at the LHC," *Physical Review D: Particles, Fields, Gravitation and Cosmology*, vol. 87, Article ID 114007, 2013.

[17] B. C. Li, Y. Y. Fu, E. Q. Wang, L. L. Wang, and F. H. Liu, "Transverse momentum dependence of charged and strange hadron elliptic flows in Cu–Cu collisions," *Journal of Physics G: Nuclear and Particle Physics*, vol. 39, no. 8, Article ID 025009, 2012.

[18] S. Andringa, E. Arushanova, and S. Asahi, "Current status and future prospects of the SNO+ experiment," *Advances in High Energy Physics*, vol. 2016, Article ID 6194250, 21 pages, 2016.

[19] B.-C. Li, Y.-Z. Wang, F.-H. Liu, X.-J. Wen, and Y.-E. Dong, "Particle production in relativistic pp and AA collisions at RHIC and LHC energies with Tsallis statistics using the two-cylindrical multisource thermal model," *Physical Review D: Particles, Fields, Gravitation and Cosmology*, vol. 89, Article ID 054014, 2014.

[20] B. C. Li, Y. Z. Wang, and F. H. Liu, "Formulation of transverse mass distributions in Au–Au collisions at $\sqrt{s}$NN = 200 GeV/nucleon," *Physics Letters B*, vol. 725, no. 4-5, pp. 352–356, 2013.

[21] B.-C. Li, Z. Zhang, J.-H. Kang, G.-X. Zhang, and F.-H. Liu, "Tsallis statistical interpretation of transverse momentum spectra in high-energy pA collisions," *Advances in High Energy Physics*, vol. 2015, Article ID 741816, 10 pages, 2015.